Nano Research

ISSN 1998-0124 CN 11-5974/O4
https://doi.org/10.1007/s12274-021-4065-9

Research Article

Detection of weak non-covalent cation-π interactions in NGAL by single-molecule force spectroscopy

Jingyuan Nie, Yibing Deng, Fang Tian, Shengchao Shi, and Peng Zheng (✉)

State Key Laboratory of Coordination Chemistry, Chemistry and Biomedicine Innovation Center (ChemBIC), School of Chemistry and Chemical Engineering, Nanjing University, 163 Xianlin Road, Nanjing 210023, China

© Tsinghua University Press and Springer-Verlag GmbH Germany, part of Springer Nature 2021

Received: 5 October 2021 / **Revised:** 23 November 2021 / **Accepted:** 9 December 2021

ABSTRACT

Cation-π interaction is an electrostatic interaction between a cation and an electron-rich arene. It plays an essential role in many biological systems as a vital driving force for protein folding, stability, and receptor-ligand interaction/recognition. To date, the discovery of most cation-π interactions in proteins relies on the statistical analyses of available three-dimensional (3D) protein structures and corresponding computational calculations. However, their experimental verification and quantification remain sparse at the molecular level, mainly due to the limited methods to dynamically measure such a weak non-covalent interaction in proteins. Here, we use atomic force microscopy-based single-molecule force spectroscopy (AFM-SMFS) to measure the stability of protein neutrophil gelatinase-associated lipocalin (also known as NGAL, siderocalin, lipocalin 2) that can bind iron through the cation-π interactions between its three cationic residues and the iron-binding tri-catechols. Based on a site-specific cysteine engineering and anchoring method, we first characterized the stability and unfolding pathways of apo-NGAL. Then, the same NGAL but bound with the iron-catechol complexes through the cation-π interactions as a holo-form was characterized. AFM measurements demonstrated stronger stabilities and kinetics of the holo-NGAL from two pulling sites, F122 and F133. Here, NGAL is stretched from the designed cysteine close to the cationic residues for a maximum unfolding effect. Thus, our work demonstrates high-precision detection of the weak cation-π interaction in NGAL.

KEYWORDS

cation–π interaction, neutrophil gelatinase-associated lipocalin (NGAL), single-molecule force spectroscopy, atomic force microscopy (AFM)

1 Introduction

Cation-π interaction is a non-covalent interaction that presents between a positively charged cation and negatively charged electron-rich π systems (Fig. 1(a)) [1, 2]. It is found ubiquitously in proteins, in which the charged side chain of residues such as Lys and Arg can be the cation, and Phe, Tyr, and Trp can be the π systems. As an electrostatic interaction in nature, the energy of a cation-π interaction is comparable to a single hydrogen bond (2–5 kcal·mol^{-1}) and is now recognized as an indispensable driving force for protein folding, stability, and receptor-ligand interaction [3–8]. One of the prominent examples is the binding of the neurotransmitter, acetylcholine, to its receptor [9]. To date, most cation-π interactions in proteins are predicted/discovered by statistical analyses of available three-dimensional protein structures using well-designed programs and computational calculations [2, 10–12]. However, their experimental verification and quantification remain limited [13–15] due to the inability to measure the small difference with high precision.

To meet this challenge, we used atomic force microscopy-based single-molecule force spectroscopy (AFM-SMFS) to measure the stability of protein neutrophil gelatinase-associated lipocalin (NGAL) containing the cation-π interactions. SMFS, such as single-molecule AFM, optical and magnetic tweezers, can mechanically manipulate one bio-macromolecule by stretching it from two well-defined points and measuring its corresponding stability [16–27]. For example, AFM-SMFS has been widely used to study protein mechanics and proteins bound with metal cofactors [28–42]. The strong ligand binding effect on proteins has also been revealed by AFM [43–45]. Moreover, the effect of another electrostatic interaction, the repulsive interaction between two positively charged imidazole rings in protein GB1, has been demonstrated by AFM [46, 47]. Thus, we combined the recently-developed high-precision AFM measurement configuration and cysteine engineering method to detect the much weaker cation-π interactions in a protein system [48–58].

In this work, NGAL was chosen as the model protein system. Structurally, NGAL has a characteristic cup-shaped calyx/cavity formed by eight-stranded antiparallel β-sheets, which can bind several macromolecular ligands (Fig. 1(b)) [59]. For example, it binds the bacterial siderophore, ferric-bound enterobactin (Fe-Ent) via simple ionic and cation-π interaction. With a sub-nanomolar K_d value, it sequesters catecholate-type siderophores from bacteria and prevents bacterial growth. Here, the cation-π interactions are present between the negatively charged Fe-Ent complex and the positively charged lysine 125, 134, and arginine 81 in the calyx. Moreover, recent studies found that a simple endogenous ligand, catechol, also chelates iron as a tri-catechol-iron complex binding to the calyx with similar cation-π interactions (Fig. 1(c)) [60]. Catechol binds to iron and forms a di-catechol species as the predominant species at pH 7.4. When

Address correspondence to pengz@nju.edu.cn

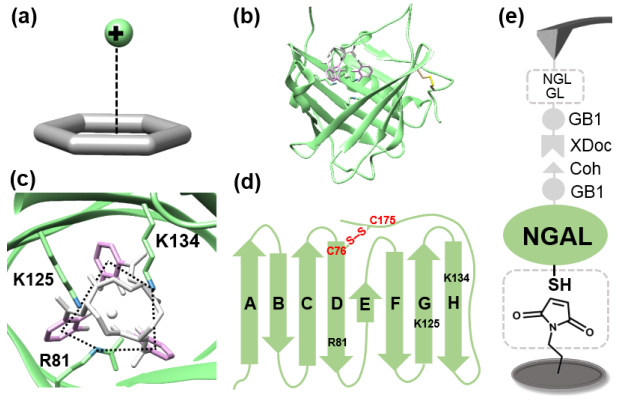

Figure 1 Schematic diagram of cation-π interactions in NGAL detected by high-precision AFM-SMFS. (a) Schematic diagram showing a cation-π interaction between a positive charge and an arene. (b) The β-barrel structured NGAL binds to enterobactin (Ent) in its cup-shaped calyx (PDB: 3CMP). (c) The enlarged view shows the cation-π interactions (dash lines) between charged residues, R81, K125, K134, and the benzene ring (colored in pink) from Ent. (d) Two-dimensional topology diagram of NGAL showing the eight stranded β-barrel structure, in which β-strands D–H containing the three cationic residues are locked by a disulfide bond (C76–C175). (e) The setup of the AFM experiment shows that the polyprotein Coh-GB1-NGAL is reacted to a maleimide-functionalized coverslip by the designed cysteine in NGAL. Then, it is picked up by the GL-GB1-XDoc-coated AFM tip, forming an [XDoc-Coh] interaction. Thus, the NGAL is stretched between the N-terminus and the designed cysteine during AFM measurement.

NGAL is further added to the solution, a tri-catechol-iron complex will form and bind to NGAL, showing a shift of maximum absorption wavelength from 575 to 498 nm. This protein represents a new type of molecular recognition utilizing cation-π interaction for iron-binding in circulation and is potentially involved with the microbial–host interface [61]. Thus, we chose this physiologically important protein to detect cation-π interactions by AFM-SMFS.

2 Experimental section

2.1 Protein engineering

The genes encoding the NGAL mutants (F122C and F133C) were obtained by site-directed mutagenesis techniques utilizing wild-type NGAL gene as the template. The constructs of protein Cohesin-GB1-NGAL (Coh-GB1-NGAL) (F122C or F133C) contain an engineered internal cysteine to immobilize the protein on the maleimide-coated glass coverslip by the reaction between sulfhydryl and maleimide group. The gene was then constructed in expression vector pQE80L using well-established standard molecular biology techniques and was confirmed by direct deoxyribonucleic acid (DNA) sequencing. All plasmids were transformed into the *Escherichia coil* (*E. coli*) strain BL21 (DE3). Bacteria were cultured in Luria–Bertani (LB) medium with 100 μg·mL^{-1} ampicillin sodium salt at 37 °C and induced by isopropyl-beta-D-thiogalactopyranoside (IPTG) with a final concentration of 1 mM.

2.2 AFM-SMFS experiments

The single-molecule force spectroscopy experiments utilized well-established standard chemical modification strategies, ensuring that the proteins of interest were completely stretched. Before the AFM experiments, GL-GB1-Xmodule-dockerin (GL-GB1-XDoc) was covalently immobilized on the tip by asparaginyl ligase *Oa*AEP1(Cys274Ala). And the protein Coh-GB1-NGAL was connected to the glass coverslip by the reaction between sulfhydryl and maleimide.

The AFM experiments were carried out on the NanoWizard4 atomic force microscope (JPK, Germany). The AFM tips (MLCT-BIO, Bruker) were calibrated in TBS buffer (20 mM Tris, 150 mM NaCl, pH 7.4) by the equipartition theorem [62]. The tip approached the substrate under a contact force of ~ 0.2 pN. The extension velocity was 400 nm·s^{-1} for the data in Figs. 2 and 3. And their acquisition sampling rate was above 7,000 Hz. For different loading rate experiments, the AFM tip was withdrawn at constant speeds ranging from 200 to 2,000 nm·s^{-1}. After recording every force-extension curve, the tip moved horizontally by 50 nm for the subsequent measurement. Six AFM cantilevers were used for successful experiments. The spring constant of them used for NGAL(F133C-apo) were ~ 39 and ~ 92 pN·nm^{-1}, for NGAL(F133C-holo) was ~ 34 pN·nm^{-1}, for NGAL(F122C-apo) were ~ 26 and ~ 48 pN·nm^{-1}, and for NGAL(F122C-holo) were ~ 109 and ~ 37 pN·nm^{-1}.

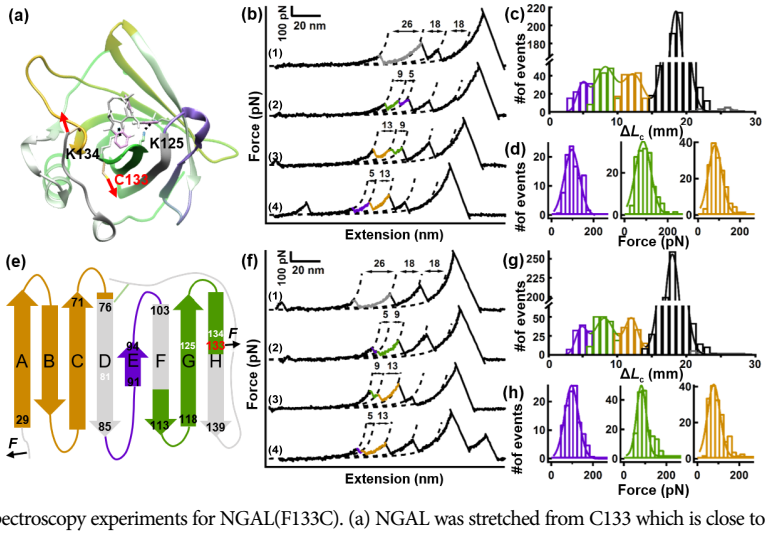

Figure 2 Single-molecule force spectroscopy experiments for NGAL(F133C). (a) NGAL was stretched from C133 which is close to the cationic residues K134. (b)–(e) Force–extension curves from apo-NGAL(F133C) show four different unfolding pathways from the extension of different β-strands of NGAL with different forces. The single peak with ΔL_c of 26 nm is from the one-step unfolding of NGAL (curve (1), colored in gray). The 5 nm-length peak (in purple) is from the extension of β-strand G–H. The 9 nm-peak (green) is from β-strand D–E, and the 12 nm-peak (khaki) is from β-strand A–C. Statistical analysis of ΔL_c histogram (c) shows four different types of peaks with ΔL_c of 5.4 ± 1.1, 8.6 ± 2.0, 12.8 ± 2.1, and 19.0 ± 1.9 nm. (f)–(h) Force–extension curves from holo-NGAL(F133C) show the same unfolding pathways as apo-form with similar unfolding forces. Statistical analysis of ΔL_c histogram (g) shows similar peaks with ΔL_c of 5.2 ± 1.2, 8.6 ± 2.1, 12.5 ± 1.4, and 18.4 ± 2.0 nm.

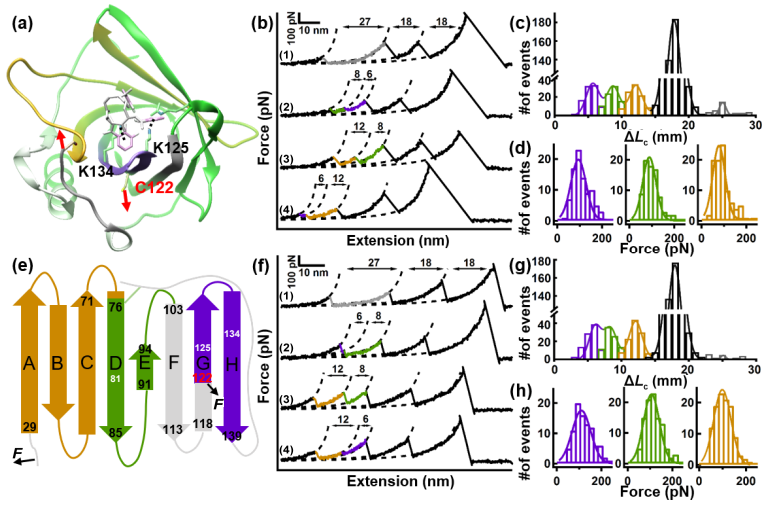

Figure 3 Single-molecule force spectroscopy experiments for NGAL(F122C). (a) NGAL was stretched from C122 close to the cationic residue K125. (b)–(e) Force–extension curves from apo-NGAL(F122C) show four similar different unfolding pathways. The single peak with ΔL_c of 27 nm is from the one-step unfolding of NGAL (curve (1), colored in gray). The 6 nm-length peak (purple) is from the extension of β-strand G–H. The 8 nm-peak (green) is from β-strand D–E, and the 12 nm-peak (khaki) is from β-strand A–C. Statistical analysis of ΔL_c histogram (c) shows four different types of peaks with ΔL_c of 6.0 ± 1.2, 8.8 ± 1.1, 12.6 ± 1.4, and 19.0 ± 1.9 nm. (f)–(h) Force–extension curves from holo-NGAL(F122C) show the same unfolding pathways as apo-form but with different unfolding forces. Statistical analysis of ΔL_c histogram (g) shows peaks with similar ΔL_c of 6.4 ± 0.9, 8.4 ± 1.1, 12.75 ± 1.4, and 18.2 ± 1.5 nm.

Finally, the force-extension curves were fitted by the worm-like chain (WLC) model (Eq. (1)) [63]. Only curves containing two unfolding signals of fingerprint GB1 and a high rupture force from the break of [XDoc-Coh] interaction were selected for analysis

$$F(x) = \frac{k_B T}{P}\left[\frac{1}{4}\left(1-\left(\frac{x}{L_c}\right)^{-2}-\frac{1}{4}+\frac{x}{L_c}\right)\right] \quad (1)$$

where P is the abbreviation for the persistence length. L_c is the contour length of the polymer/protein. T is the absolute temperature in kelvin. k_B is the Boltzmann constant.

We applied the Savitzky–Golay filter to smooth all the curves during data analysis and presentation. The smoothing width was 13. The filter can reduce high-frequency noise to improve the accuracy of data without changing the signal trend.

2.3 Chemical modifications of AFM tips and glass substrate

Si_3N_4 AFM tips (MLCT-BIO, Bruker) and coverslip were cleaned by plasma treatment and silanized, incubated with 3-aminopropyltriethoxysilane (APTES) away from light to introduce amine groups. Then the tips and cover glasses were incubated with azidation reacting solution (4 mM $ImSO_2N_3$, 8 mM K_2CO_3, and 40 μM $CuSO_4$) at room temperature to introduce azide group. After azidation, the tips and cover glasses were incubated with 2 mM DBCO-$(PEG)_4$-maleimide solution for 1 h at 37 °C in order to introduce maleimide groups on the surface. Finally, the maleimide-coated tips were cleaned with ultrapure water and incubated with Cys-ELP_{20}-NGL. After incubation with the ELP_{20}, tips were cleaned and stored at 4 °C before measurement. The maleimide-coated cover glasses were stored in a vacuum environment to prevent the maleimide group from being hydrolyzed.

3 Results and discussion

Typically, the target protein is stretched and unfolded from its N and C terminus by AFM-SMFS because the protein is immobilized by these two sites between the AFM tip and coverslip. However, the area for cation-π interactions in NGAL is "locked" by an endogenous disulfide bond (Cys76 to Cys175, Figs. 1(b) and 1(d)) which is mechanostable and cannot be broken during AFM measurement [64]. We introduced one cysteine close to the cationic residues as the internal pulling site to solve this problem [65]. This cysteine will react to the maleimide-coated coverslip used, leading to protein immobilization. Thus, the protein will be stretched between this cysteine and the N-terminus (Fig. 1(e)). As a result, the area for cation-π interactions can be probed during NGAL unfolding. Moreover, the pulling site is very close to the cationic residue, which may maximize the effect of cation-π interaction for NGAL unfolding and lead to the detection of this weak interaction.

To achieve a high-precision AFM-SMFS measurement and detection of the weak cation-π interactions in NGAL, a polyprotein, namely, Coh-GB1-NGAL(Cys) was designed. It allows the stretch of NGAL between the designed cysteine and its N-terminus (Fig. 1(e)). Coh was added for an efficient protein pick-up by the AFM tip, on which another polyprotein XDoc-GB1 is functionalized enzymatically [49, 66, 67]. When the tip is pressed on the sample-immobilized substrate, XDoc binds efficiently to Coh as a specific [XDoc-Coh] protein-protein interaction. This led to a complete force loop from the AFM tip to the coverslip, as tip-GB1-[XDoc-Coh]-GB1-NGAL(Cys)-coverslip. Then, by moving the tip up, NGAL can be stretched from its N-terminus and the cysteine and unfolded at last. Also, a marker protein GB1 with a known ΔL_c of 18 nm was added for an unambiguous single-molecule detection [68]. After all protein domains were unfolded, a characteristic high rupture peak with a force of ~ 500 pN from the break of [XDoc-Coh] could be observed. And the tip was moved to another location, and this measurement was repeated.

We first chose Phe133 as the pulling site, which is close to the cationic residue Lys134. Polyprotein Coh-GB1-NGAL(F133C) was constructed and characterized (Fig. S1 in the Electronic Supplementary Material (ESM)). Apo-NGAL without bound tri-catechol-iron complex was measured first to understand its unfolding mechanism and signature. Stretched by single-molecule AFM, the unfolding of polyprotein resulted in a typical sawtooth-like force–extension curve with multiple peaks (Figs. 2(b)–2(d)). First, there were a few simple one-step unfolding events of NGAL (Fig. 2(b), curve (1), color in gray) with a ΔL_c of ~ 26 nm, fitted by the worm-like chain model describing the relationship between polymer elasticity and applied force [63]. Theoretically, the ΔL_c value of the complete unfolding of NGAL equals to the unfolding

of β-strands A–C, which are outside the disulfide bond (residues 29–75, 47aa × 0.36 – 2.21 = 14.7 nm), plus the short side of the disulfide bond locked circle (residues 133–175, 44aa × 0.36 – 2.6 = 12.9 nm). Thus, the theoretical ΔL_c is 27.6 nm, which agrees with the experimental value. This result indicates that NGAL was measured successfully by AFM from the designed cysteine.

In addition to the one-step unfolding event, most curves showed three different types of stepwise unfolding pathways (Fig. S3 in the ESM), including 9 + 5 (Fig. 2(b), curve (2)); 13 + 9 (curve (3)), and 5 + 13 nm (curve (4)). The 5.4 nm-length peak agrees with the unfolding of β-strand E (Figs. 2(c)–2(e), colored in purple, residues 85–103, 19aa × 0.36 – 1.9 = 5.0 nm) with an average unfolding force of 97 ± 52 pN (ave. ± stdv., n = 100) (Tables 1 and 2, and Table S1 in the ESM). The 8.6 nm-length peak agrees with the unfolding of β-strands G and partial F and H containing the cation residue K125 (in green, n = 161, residues 107–133, 27aa × 0.36 – 0.92 = 8.8 nm). The force was 86 ± 50 pN. And the 12.8 nm-length peak agrees with the unfolding of β-strands A–C (in khaki, n = 162, residues 29–75, 47aa × 0.36 – 2.2 = 14.7 nm) with a force of 82 ± 48 pN.

Next, we performed the experiment on the holo-NGAL(F133C) bound with the tri-catechol-iron complex. Ultraviolet–visible (UV–vis) spectrum of this mutant showed the same result as WT-NGAL with the characteristic signal at 498 nm due to the complex binding (Fig. S2 in the ESM). As a result, the cysteine mutation does not affect the property of NGAL, especially its binding to the complex. Then, we performed the AFM-SMFS experiment on polyprotein Coh-GB1-holo-NGAL(F133C). Similarly, it showed all the same unfolding pathways previously observed for the apo-NGAL(F133C) (Figs. 2(f) and 2(g)), indicating that the complex binding does not affect the unfolding pathway of NGAL and thus has a weak effect for NGAL. Moreover, we found that the unfolding forces of the holo-form are similar to the apo-form for each peak (Fig. 2(h) and Table 1). The unfolding force is 97 ± 48 pN (n = 109) for the 5-nm peak, 82 ± 48 pN (n = 174) for the 9 nm-peak and 79 ± 48 pN for the 13 nm peak (n = 168) (Fig. 2(h) and Table 1). This constant-speed pulling AFM unfolding experiment suggests that the complex binding due to the cation-π interactions only has a very small effect for NGAL when pulled from residue 133 site.

To further test whether AFM-SMFS can detect the effect of such a weak cation-π interaction for NGAL, we chose Phe122 as another pulling site close to the cationic residue Lys125. Polyprotein Coh-GB1-NGAL(F122C) was constructed. A similar AFM measurement was performed on apo-NGAL(F122C) and yielded a similar unfolding pathway with a slightly different length (Figs. 3(b) and 3(c)). First, there were also a few one-step unfolding events of NGAL (Fig. 3(b), curve (1)) with a ΔL_c of ~ 27 nm. This value agrees with the theoretical value of unfolding of NGAL (29.1 nm) when stretched between Cys122 and the N-terminus. The first part is the unfolding of β-strands A–C outside the disulfide bond (residues 29–75, 47aa × 0.36 – 2.21 = 14.7 nm). And the second is the short side of the disulfide bond locked circle (residues 76–122, 47 aa × 0.36 – 2.5 = 14.4 nm).

Similarly, most curves show three different stepwise unfolding pathways, including 8 + 6 (Fig. 3(b), curve (2)), 12 + 8 (curve (3)), and 6 + 12 mm (curve (4)). The 8.8 nm-length peak agrees with the unfolding of β-strands D–E (Fig. 3(c)–3(e), color in green, n = 79, residues 76–102, 27aa × 0.36 – 2.6 = 7.1 nm) with an average unfolding force of 88 ± 42 pN. The 6.0 nm-length peak agrees with the unfolding of β-strands G–H containing the two positively charged residues K125 and K134 (in purple, n = 89, residues 122–139, 18aa × 0.36 – 1.5 = 5.0 nm) with a force of 94 ± 48 pN. The 12.6 nm-length peak agrees with the unfolding of β-strands A–C (in khaki, n = 94, residues 29–75, 47aa × 0.36 – 2.21 = 14.7 nm) with a force of 77 ± 38 pN.

Then, we performed the AFM-SMFS experiment on the holo-NGAL(F122C). All similar unfolding pathways were observed (Figs. 3(f) and 3(g), Figs. S1 and S2 in the ESM). Most importantly, we found that the unfolding force of each peak showed a modest increment of ~ 20 pN, which is a 15% increase (Fig. 3(h) and Table 1, and Fig. S4 in the ESM). This result indicates that the complex binding due to the cation-π interactions stabilizes the NGAL and is detected by AFM-SMFS.

Consequently, we continued the AFM measurements to obtain the unfolding kinetics of both mutants for further comparison. The AFM unfolding experiments of the two NGAL mutants in the presence or not of the complex were performed under different pulling speeds (Fig. S5 in the ESM). And the unfolding force of the protein was dependent on the logarithm of force loading rate (Fig. 4). Fitted by the Bell–Evans model, Δx and off rates k_{off} for each unfolding step can be obtained (Table 2). This time, clear differences between the kinetics were observed. All unfolding steps from holo-NGAL showed a smaller k_{off} compared with the apo-NGAL, indicating that cation-π interaction stabilized the structure of NGAL.

In this work, we experimentally detected and quantified the weak yet essential cation-π interaction in a protein system at the molecular level, using the recently developed high-precision AFM-SMFS system and cysteine immobilization method. Most of the discovery of cation-π interactions in proteins has come from the statistical analyses of protein structure databases and corresponding computational calculations. Quite a few well-developed programs have been used to identify this

Table 1 The unfolding force of NGAL by AFM-SMFS

	ΔL_c (nm)	F (apo, pN)	F (holo, pN)
F133C	5	97 ± 52	97 ± 48
	9	86 ± 50	82 ± 48
	13	82 ± 48	79 ± 42
F122C	6	94 ± 48	110 ± 59
	8	88 ± 42	106 ± 50
	12	77 ± 38	99 ± 52

Table 2 AFM-SMFS results of NGALs

	ΔL_c (nm)	Apo		ΔLc (nm)	Holo	
		Δx (nm)	k_{off} (s^{-1})		Δx (nm)	k_{off} (s^{-1})
F133C	5.4 ± 1.1	0.18	2.6	5.2 ± 1.2	0.23	1.4
	8.6 ± 2.0	0.18	3.3	8.6 ± 2.1	0.24	1.7
	12.8 ± 2.1	0.19	3.8	12.5 ± 1.4	0.24	1.6
F122C	6.0 ± 1.2	0.16	3.7	6.4 ± 0.9	0.22	0.9
	8.8 ± 1.1	0.18	2.5	8.4 ± 1.1	0.21	1.0
	12.6 ± 1.4	0.22	2.3	12.7 ± 1.4	0.21	1.3

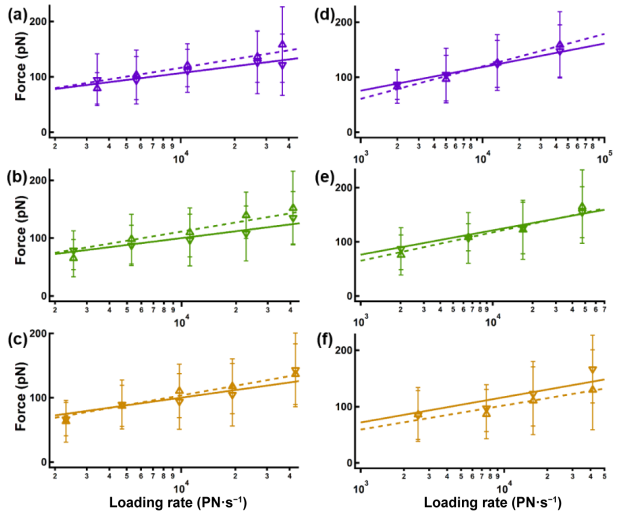

Figure 4 The plot between the logarithm of loading rate and rupture force of NGAL shows a linear relationship. (a)–(c) The loading rate experiment of NGAL(F133C) showed a different result upon the binding of the complex for each force peak ((a): colored in purple for 5 nm, (b): green for 9 nm, and (c): khaki for 13 nm). The dashed line is for apo-form, and the solid line is for holo-form. (d)–(f) Similar results were obtained for NGAL(F122C).

interaction based on the geometry or energy between two possible sites in a protein [2, 3, 6]. Nevertheless, an experimental verification was necessary to verify its presence further, especially at the molecular level. Here, our AFM-SMFS measurement directly provides the force value for the effect and its kinetic information.

It is noted that the strength of the effect of cation-π interactions for NGAL was weak from our AFM measurement. The mutant (F122C) only showed a modest force increase (~ 20 pN). Although the effect for the kinetics is more obvious, only two times the k_{off} difference was observed for most unfolding events. In contrast, the electrostatic repulsion effect from the two positive charge histidine residues for protein GB1 is much more significant [46]. The stability of the GB1 mutant decreases by 65 pN, and its k_{off} decreases ~ 5 times. And many other studies revealed a strong ligand binding effect for protein (un)folding, such as the binding of calcium on calmodulin folding [43, 44]. Here, our result showed a weaker effect upon the complex binding. In AFM measurement, typically only a hydrogen bond network containing several hydrogen bonds, such as β-sheet, showed a detectable change of force. However, the energy of a cation-π interaction is only 2–5 kcal·mol^{-1}, similar to one/two hydrogen bonds.

Another interesting point is the different effects of cation-π interactions for NGAL unfolding when pulled from different sites. Compared to NGAL(F122C) results, NGAL(F133C) even did not show a detectable unfolding force difference. To further understand the mechanism, we performed simple steered molecular dynamics (SMD) simulations for the unfolding of the two mutants without the complex binding. The results indicated that the F122C showed a much higher force peak upon the unfolding of the residues involving the cation-π interaction (Fig. S6 in the ESM). Consequently, the cation-π interaction may play a more direct and important role upon the unfolding energy barrier of NGAL(F122C) and showed a more different unfolding force upon the complex binding.

Finally, our work also provides an updated method to stretch protein from a designed cysteine site using the cysteine-maleimide chemistry [65, 69]. Several previous AFM works have shown the anisotropic mechanical stability of protein when pulled from different sites using the cysteine engineering methods, such as ubiquitin, GFP, and rubredoxin [29, 69, 70]. There, the engineered cysteine is mainly used for protein coupling and thus determines the direction of force propagation. Here for NGAL, the reducing agent, which is usually added to break the formation of the self-disulfide bond between protein monomers was not added to avoid the break of the endogenous disulfide bond. Nevertheless, using a maleimide-coated coverslip or surface, only unoxidized NGAL monomer with the free cysteine can immobilize, forming stable covalent C–S bond linkage. In addition, the target protein is ready to be incorporated into the high-precision AFM system, leading to a more efficient measurement.

4 Conclusions

In conclusion, we detected the small influence of cation-π interactions for NGAL experimentally by high-precision AFM-SMFS and cysteine-mediated site-specific protein immobilization. Combined with the classic theoretical and computational methods, we believe the mechanism of this essential cation-π interaction for protein can be more revealed.

Acknowledgments

This work was funded by the Fundamental Research Funds for the Central Universities (No. 14380259), Natural Science Foundation of Jiangsu Province (No. BK20200058), the National Natural Science Foundation of China (Nos. 21771103 and 21977047), and computational resources from computing facilities of the High-Performance Computing Center (HPCC) of Nanjing University.

Electronic Supplementary Material: Supplementary material (additional SDS-PAGE, UV–vis, protein sequences, and more experimental methods) is available in the online version of this article at https://doi.org/10.1007/s12274-021-4065-9.

References

[1] Ma, J. C.; Dougherty, D. A. The cation-π interaction. *Chem. Rev.* **1997**, *97*, 1303–1324.

[2] Kumar, K.; Woo, S. M.; Siu, T.; Cortopassi, W. A.; Duarte, F.; Paton, R. S. Cation-π interactions in protein-ligand binding: Theory and data-mining reveal different roles for lysine and arginine. *Chem. Sci.* **2018**, *9*, 2655–2665.

[3] Mahadevi, A. S.; Sastry, G. N. Cation-π interaction: Its role and relevance in chemistry, biology, and material science. *Chem. Rev.* **2013**, *113*, 2100–2138.

[4] Shigedomi, K.; Osada, S.; Jelokhani-Niaraki, M.; Kodama, H. Systematic design and validation of ion channel stabilization of amphipathic α-helical peptides incorporating tryptophan residues. *ACS Omega* **2021**, *6*, 723–732.

[5] Dougherty, D. A. The cation-π interaction. *Acc. Chem. Res.* **2013**, *46*, 885–893.

[6] Waheed, Q.; Khan, H. M.; He, T.; Roberts, M.; Gershenson, A.; Reuter, N. Interfacial aromatics mediating cation-π interactions with choline-containing lipids can contribute as much to peripheral protein affinity for membranes as aromatics inserted below the phosphates. *J. Phys. Chem. Lett.* **2019**, *10*, 3972–3977.

[7] Wang, Q.; Li, R.; Ouyang, X.; Wang, G. J. A novel indole-based conjugated microporous polymer for highly effective removal of heavy metals from aqueous solution via double cation-π interactions. *RSC Adv.* **2019**, *9*, 40531–40535.

[8] Crowley, P. B.; Golovin, A. Cation-π interactions in protein-protein interfaces. *Proteins: Struct., Funct. Bioinformatics* **2005**, *59*, 231–239.

[9] Dougherty, D. A.; Stauffer, D. A. Acetylcholine binding by a synthetic receptor: Implications for biological recognition. *Science* **1990**, *250*, 1558–1560.

[10] Zheng, W. W.; Dignon, G. L.; Jovic, N.; Xu, X. C.; Regy, R. M.; Fawzi, N. L.; Kim, Y. C.; Best, R. B.; Mittal, J. Molecular details of protein condensates probed by microsecond long atomistic simulations. *J. Phys. Chem. B* **2020**, *124*, 11671–11679.
[11] Singh, V. B. Spectroscopic signatures and the cation-π interaction in conformational preferences of the neurotransmitter dopamine in aqueous solution. *ACS Chem. Neurosci.* **2021**, *12*, 613–625.
[12] Boknevitz, K.; Darrigan, C.; Chrostowska, A.; Liu, S. Y. Cation-π binding ability of BN indole. *Chem. Commun.* **2020**, *56*, 3749–3752.
[13] Gebbie, M. A.; Wei, W.; Schrader, A. M.; Cristiani, T. R.; Dobbs, H. A.; Idso, M.; Chmelka, B. F.; Waite, J. H.; Israelachvili, J. N. Tuning underwater adhesion with cation-π interactions. *Nat. Chem.* **2017**, *9*, 473–479.
[14] Prampolini, G.; d'Ischia, M.; Ferretti, A. The phenoxyl group-modulated interplay of cation-π and σ-type interactions in the alkali metal series. *Phys. Chem. Chem. Phys.* **2020**, *22*, 27105–27120.
[15] Pinheiro, S.; Soteras, I.; Gelpí, J. L.; Dehez, F.; Chipot, C.; Luque, F. J.; Curutchet, C. Structural and energetic study of cation-π-cation interactions in proteins. *Phys. Chem. Chem. Phys.* **2017**, *19*, 9849–9861.
[16] Rivas-Pardo, J. A.; Li, Y.; Mártonfalvi, Z.; Tapia-Rojo, R.; Unger, A.; Fernández-Trasancos, Á.; Herrero-Galán, E.; Velázquez-Carreras, D.; Fernández, J. M.; Linke, W. A. et al. A HaloTag-TEV genetic cassette for mechanical phenotyping of proteins from tissues. *Nat. Commun.* **2020**, *11*, 2060.
[17] Le, S. M.; Yu, M.; Yan, J. Direct single-molecule quantification reveals unexpectedly high mechanical stability of vinculin-talin/α-catenin linkages. *Sci. Adv.* **2019**, *5*, eaav2720.
[18] Hoffer, N. Q.; Neupane, K.; Pyo, A. G. T.; Woodside, M. T. Measuring the average shape of transition paths during the folding of a single biological molecule. *Proc. Natl. Acad. Sci. USA* **2019**, *116*, 8125–8130.
[19] Dahal, N.; Nowitzke, J.; Eis, A.; Popa, I. Binding-induced stabilization measured on the same molecular protein substrate using single-molecule magnetic tweezers and heterocovalent attachments. *J. Phys. Chem. B* **2020**, *124*, 3283–3290.
[20] Wolny, M.; Batchelor, M.; Bartlett, G. J.; Baker, E. G.; Kurzawa, M.; Knight, P. J.; Dougan, L.; Woolfson, D. N.; Paci, E.; Peckham, M. Characterization of long and stable *de novo* single alpha-helix domains provides novel insight into their stability. *Sci. Rep.* **2017**, *7*, 44341.
[21] Zhang, X. X.; Chen, J. L.; Li, E. C.; Hu, C. G.; Luo, S. Z.; He, C. Z. Ultrahigh adhesion force between silica-binding peptide SB7 and glass substrate studied by single-molecule force spectroscopy and molecular dynamic simulation. *Front. Chem.* **2020**, *8*, 600918.
[22] Li, J. Q.; Wijeratne, S. S.; Nelson, T. E.; Lin, T. C.; He, X.; Feng, X. W.; Nikoloutsos, N.; Fang, R.; Jiang, K.; Lian, I. et al. Dependence of membrane tether strength on substrate rigidity probed by single-cell force spectroscopy. *J. Phys. Chem. Lett.* **2020**, *11*, 4173–4178.
[23] Paul, D.; Roy, A.; Nandy, A.; Datta, B.; Borar, P.; Pal, S. K.; Senapati, D.; Rakshit, T. Identification of biomarker hyaluronan on colon cancer extracellular vesicles using correlative afm and spectroscopy. *J. Phys. Chem. Lett.* **2020**, *11*, 5569–5576.
[24] Brückner, S.; Schubert, R.; Kraushaar, T.; Hartmann, R.; Hoffmann, D.; Jelli, E.; Drescher, K.; Müller, D. J.; Essen, L. O.; Mösch, H. U. Kin discrimination in social yeast is mediated by cell surface receptors of the Flo11 adhesin family. *Elife* **2020**, *9*, e55587.
[25] Schönfelder, J.; Alonso-Caballero, A.; De Sancho, D.; Perez-Jimenez, R. The life of proteins under mechanical force. *Chem. Soc. Rev.* **2018**, *47*, 3558–3573.
[26] Xiang, W. T.; Li, Z. D.; Xu, C. Q.; Li, J.; Zhang, W. K.; Xu, H. P. Quantifying the bonding strength of gold-chalcogen bonds in block copolymer systems. *Chem.—Asian J.* **2019**, *14*, 1481–1486.
[27] Zhao, P.; Xu, C. Q.; Sun, C. X.; Xia, J. H.; Sun, L.; Li, J.; Xu, H. P. Exploring the difference of bonding strength between silver(I) and chalcogenides in block copolymer systems. *Polym. Chem.* **2020**, *11*, 7087–7093.
[28] Hoffmann, T.; Tych, K. M.; Crosskey, T.; Schiffrin, B.; Brockwell, D. J.; Dougan, L. Rapid and robust polyprotein production facilitates single-molecule mechanical characterization of β-barrel assembly machinery polypeptide transport associated domains. *ACS Nano* **2015**, *9*, 8811–8821.
[29] Brockwell, D. J.; Paci, E.; Zinober, R. C.; Beddard, G. S.; Olmsted, P. D.; Smith, D. A.; Perham, R. N.; Radford, S. E. Pulling geometry defines the mechanical resistance of a β-sheet protein. *Nat. Struct. Mol. Biol.* **2003**, *10*, 731–737.
[30] Müller, D. J.; Dumitru, A. C.; Lo Giudice, C.; Gaub, H. E.; Hinterdorfer, P.; Hummer, G.; De Yoreo, J. J.; Dufrêne, Y. F.; Alsteens, D. Atomic force microscopy-based force spectroscopy and multiparametric imaging of biomolecular and cellular systems. *Chem. Rev.* **2021**, *121*, 11701–11725.
[31] Scholl, Z. N.; Li, Q.; Yang, W. T.; Marszalek, P. E. Single-molecule force spectroscopy reveals the calcium dependence of the alternative conformations in the native state of β, γ-crystallin protein. *J. Biol. Chem.* **2016**, *291*, 18263–18275.
[32] Rico, F.; Russek, A.; González, L.; Grubmüller, H.; Scheuring, S. Heterogeneous and rate-dependent streptavidin-biotin unbinding revealed by high-speed force spectroscopy and atomistic simulations. *Proc. Natl. Acad. Sci. USA* **2019**, *116*, 6594–6601.
[33] Zheng, P.; Li, H. B. Highly covalent ferric-thiolate bonds exhibit surprisingly low mechanical stability. *J. Am. Chem. Soc.* **2011**, *133*, 6791–6798.
[34] Yuan, G. D.; Liu, H. X.; Ma, Q.; Li, X.; Nie, J. Y.; Zuo, J. L.; Zheng, P. Single-molecule force spectroscopy reveals that iron-ligand bonds modulate proteins in different modes. *J. Phys. Chem. Lett.* **2019**, *10*, 5428–5433.
[35] Song, G. B.; Ding, X.; Liu, H. X.; Yuan, G. D.; Tian, F.; Shi, S. C.; Yang, Y.; Li, G. Q.; Zheng, P. Single-molecule force spectroscopy reveals that the Fe-N bond enables multiple rupture pathways of the 2Fe2S cluster in a MitoNEET monomer. *Anal. Chem.* **2020**, *92*, 14783–14789.
[36] Tunn, I.; de Léon, A. S.; Blank, K. G.; Harrington, M. J. Tuning coiled coil stability with histidine-metal coordination. *Nanoscale* **2018**, *10*, 22725–22729.
[37] Infante, E.; Stannard, A.; Board, S. J.; Rico-Lastres, P.; Rostkova, E.; Beedle, A. E. M.; Lezamiz, A.; Wang, Y. J.; Breen, S. G.; Panagaki, F. et al. The mechanical stability of proteins regulates their translocation rate into the cell nucleus. *Nat. Phys.* **2019**, *15*, 973–981.
[38] Oh, Y. J.; Köhler, M.; Lee, Y.; Mishra, S.; Won Park, J.; Hinterdorfer, P. Label-free probing of binding affinity using topography and recognition imaging. *Biophys. J.* **2020**, *118*, 174a–175a.
[39] Fu, L. L.; Wang, H.; Li, H. B. Harvesting mechanical work from folding-based protein engines: From single-molecule mechanochemical cycles to macroscopic devices. *CCS Chem.* **2019**, *1*, 138–147.
[40] Perales-Calvo, J.; Lezamiz, A.; Garcia-Manyes, S. The mechanochemistry of a structural zinc finger. *J. Phys. Chem. Lett.* **2015**, *6*, 3335–3340.
[41] Freitas, F. C.; de Oliveira, R. J. Extension-dependent drift velocity and diffusion (drdiff) directly reconstructs the folding free energy landscape of atomic force microscopy experiments. *J. Phys. Chem. Lett.* **2020**, *11*, 800–807.
[42] Herman, K.; Lekka, M.; Ptak, A. Unbinding kinetics of syndecans by single-molecule force spectroscopy. *J. Phys. Chem. Lett.* **2018**, *9*, 1509–1515.
[43] Stigler, J.; Rief, M. Calcium-dependent folding of single calmodulin molecules. *Proc. Natl. Acad. Sci. USA* **2012**, *109*, 17814–17819.
[44] Pelz, B.; Žoldák, G.; Zeller, F.; Zacharias, M.; Rief, M. Subnanometre enzyme mechanics probed by single-molecule force spectroscopy. *Nat. Commun.* **2016**, *7*, 10848.
[45] Gunnoo, M.; Cazade, P. A.; Orlowski, A.; Chwastyk, M.; Liu, H. P.; Ta, D. T.; Cieplak, M.; Nash, M.; Thompson, D. Steered molecular dynamics simulations reveal the role of Ca^{2+} in regulating mechanostability of cellulose-binding proteins. *Phys. Chem. Chem. Phys.* **2018**, *20*, 22674–22680.
[46] Zheng, P.; Cao, Y.; Bu, T. J.; Straus, S. K.; Li, H. B. Single molecule force spectroscopy reveals that electrostatic interactions affect the mechanical stability of proteins. *Biophys. J.* **2011**, *100*, 1534–1541.

[47] Muddassir, M.; Manna, B.; Singh, P.; Singh, S.; Kumar, R.; Ghosh, A.; Sharma, D. Single-molecule force-unfolding of titin I27 reveals a correlation between the size of the surrounding anions and its mechanical stability. *Chem. Commun.* **2018**, *54*, 9635–9638.

[48] Yang, B.; Liu, Z. W.; Liu, H. P.; Nash, M. A. Next generation methods for single-molecule force spectroscopy on polyproteins and receptor-ligand complexes. *Front. Mol. Biosci.* **2020**, *7*, 85.

[49] Stahl, S. W.; Nash, M. A.; Fried, D. B.; Slutzki, M.; Barak, Y.; Bayer, E. A.; Gaub, H. E. Single-molecule dissection of the high-affinity cohesin-dockerin complex. *Proc. Natl. Acad. Sci. USA* **2012**, *109*, 20431–20436.

[50] Durner, E.; Ott, W.; Nash, M. A.; Gaub, H. E. Post-translational sortase-mediated attachment of high-strength force spectroscopy handles. *ACS Omega* **2017**, *2*, 3064–3069.

[51] Deng, Y. B.; Wu, T.; Wang, M. D.; Shi, S. C.; Yuan, G. D.; Li, X.; Chong, H. C.; Wu, B.; Zheng, P. Enzymatic biosynthesis and immobilization of polyprotein verified at the single-molecule level. *Nat. Commun.* **2019**, *10*, 2775.

[52] Dietz, H.; Rief, M. Protein structure by mechanical triangulation. *Proc. Natl. Acad. Sci. USA* **2006**, *103*, 1244–1247.

[53] Becke, T. D.; Ness, S.; Kaufmann, B. K.; Hartmann, B.; Schilling, A. F.; Sudhop, S.; Hilleringmann, M.; Clausen-Schaumann, H. Pilus-1 backbone protein RrgB of *streptococcus pneumoniae* binds collagen i in a force-dependent way. *ACS Nano* **2019**, *13*, 7155–7165.

[54] Xing, H.; Li, Z. D.; Wang, W. B.; Liu, P. R.; Liu, J.; Song, Y.; Wu, Z. L.; Zhang, W. K.; Huang, F. H. Mechanochemistry of an interlocked poly[2]catenane: From single molecule to bulk gel. *CCS Chem.* **2020**, *2*, 513–523.

[55] Bao, Y.; Luo, Z. L.; Cui, S. X. Environment-dependent single-chain mechanics of synthetic polymers and biomacromolecules by atomic force microscopy-based single-molecule force spectroscopy and the implications for advanced polymer materials. *Chem. Soc. Rev.* **2020**, *49*, 2799–2827.

[56] Liu, Z. W.; Moreira, R. A.; Dujmović, A.; Liu, H. P.; Yang, B.; Poma, A. B.; Nash, M. A. Mapping mechanostable pulling geometries of a therapeutic anticalin/CTLA-4 protein complex. *Nano Lett.*, in press, https://doi.org/10.1021/acs.nanolett.1c03584.

[57] Synakewicz, M.; Bauer, D.; Rief, M.; Itzhaki, L. S. Bioorthogonal protein-DNA conjugation methods for force spectroscopy. *Sci. Rep.* **2019**, *9*, 13820.

[58] Hu, X. L.; Zhao, X. Q.; He, B. Z.; Zhao, Z.; Zheng, Z.; Zhang, P. F.; Shi, X. J.; Kwok, R. T. K.; Lam, J. W. Y.; Qin, A. J. et al. A simple approach to bioconjugation at diverse levels: Metal-free click reactions of activated alkynes with native groups of biotargets without prefunctionalization. *Research* **2018**, *2018*, 3152870.

[59] Gasymov, O. K.; Abduragimov, A. R.; Glasgow, B. J. Cation-π interactions in lipocalins: Structural and functional implications. *Biochemistry* **2012**, *51*, 2991–3002.

[60] Bao, G. H.; Clifton, M.; Hoette, T. M.; Mori, K.; Deng, S. X.; Qiu, A. D.; Viltard, M.; Williams, D.; Paragas, N.; Leete, T. et al. Iron traffics in circulation bound to a siderocalin (Ngal)-catechol complex. *Nat. Chem. Biol* **2010**, *6*, 602–609.

[61] Goetz, D. H.; Holmes, M. A.; Borregaard, N.; Bluhm, M. E.; Raymond, K. N.; Strong, R. K. The neutrophil lipocalin NGAL is a bacteriostatic agent that interferes with siderophore-mediated iron acquisition. *Mol. Cell* **2002**, *10*, 1033–1043.

[62] Hutter, J. L.; Bechhoefer, J. Calibration of atomic-force microscope tips. *Rev. Sci. Instrum.* **1993**, *64*, 1868–1873.

[63] Marko, J. F.; Siggia, E. D. Stretching DNA. *Macromolecules* **1995**, *28*, 8759–8770.

[64] Ainavarapu, S. R. K.; Brujić, J.; Huang, H. H.; Wiita, A. P.; Lu, H.; Li, L.; Walther, K. A.; Carrion-Vazquez, M.; Li, H. B.; Fernandez, J. M. Contour length and refolding rate of a small protein controlled by engineered disulfide bonds. *Biophys. J.* **2007**, *92*, 225–233.

[65] Zheng, P.; Cao, Y.; Li, H. B. Facile method of constructing polyproteins for single-molecule force spectroscopy studies. *Langmuir* **2011**, *27*, 5713–5718.

[66] Tian, F.; Tong, B.; Sun, L.; Shi, S. C.; Zheng, B.; Wang, Z. B.; Dong, X. C.; Zheng, P. N501y mutation of spike protein in SARS-CoV-2 strengthens its binding to receptor ACE2. *Elife* **2021**, *10*, e69091.

[67] LeBlanc, M. A.; Fink, M. R.; Perkins, T. T.; Sousa, M. C. Type III secretion system effector proteins are mechanically labile. *Proc. Natl. Acad. Sci. USA* **2021**, *118*, e2019566118.

[68] Cao, Y.; Lam, C.; Wang, M. J.; Li, H. B. Nonmechanical protein can have significant mechanical stability. *Angew. Chem., Int. Ed.* **2006**, *45*, 642–645.

[69] Dietz, H.; Bertz, M.; Schlierf, M.; Berkemeier, F.; Bornschlogl, T.; Junker, J. P.; Rief, M. Cysteine engineering of polyproteins for single-molecule force spectroscopy. *Nat. Protoc.* **2006**, *1*, 80–84.

[70] Zheng, P.; Chou, C. C.; Guo, Y.; Wang, Y. Y.; Li, H. B. Single molecule force spectroscopy reveals the molecular mechanical anisotropy of the FeS_4 metal center in rubredoxin. *J. Am. Chem. Soc.* **2013**, *135*, 17783–17792.